

Article

Effective Separation of Prime Olefins from Gas Stream Using Anion Pillared Metal Organic Frameworks: Ideal Adsorbed Solution Theory Studies, Cyclic Application and Stability

Majeda Khraisheh ^{1,*} , Fares Almomani ¹  and Gavin Walker ²

¹ Department of Chemical Engineering, College of Engineering, Qatar University, Doha P.O. Box 2713, Qatar; falmomani@qu.edu.qa

² Department of Chemical Sciences, SSPC, Bernal Institute, University of Limerick, V94 T9PX Limerick, Ireland; Gavin.Walker@ul.ie

* Correspondence: m.khraisheh@qu.edu.qa

Abstract: The separation of C_3H_4/C_3H_6 is one of the most energy intensive and challenging operations, requiring up to 100 theoretical stages, in traditional cryogenic distillation. In this investigation, the potential application of two MOFs (SIFSIX-3-Ni and NbOFFIVE-1-Ni) was tested by studying the adsorption-desorption behaviors at a range of operational temperatures (300–360 K) and pressures (1–100 kPa). Dynamic adsorption breakthrough tests were conducted and the stability and regeneration ability of the MOFs were established after eight consecutive cycles. In order to establish the engineering key parameters, the experimental data were fitted to four isotherm models (Langmuir, Freundlich, Sips and Toth) in addition to the estimation of the thermodynamic properties such as the isosteric heats of adsorption. The selectivity of the separation was tested by applying ideal adsorbed solution theory (IAST). The results revealed that SIFSIX-3-Ni is an effective adsorbent for the separation of 10/90 *v/v* C_3H_4/C_3H_6 under the range of experimental conditions used in this study. The maximum adsorption reported for the same combination was 3.2 mmol g^{-1} . Breakthrough curves confirmed the suitability of this material for the separation with a 10-min gap before the lighter C_3H_4 is eluted from the column. The separated C_3H_6 was obtained with a 99.98% purity.

Keywords: metal organic frame works; olefin paraffin separations; propyne; propylene; adsorption isotherms; dynamic breakthrough



Citation: Khraisheh, M.; Almomani, F.; Walker, G. Effective Separation of Prime Olefins from Gas Stream Using Anion Pillared Metal Organic Frameworks: Ideal Adsorbed Solution Theory Studies, Cyclic Application and Stability. *Catalysts* **2021**, *11*, 510. <https://doi.org/10.3390/catal11040510>

Academic Editor: Jorge Bedia

Received: 7 March 2021

Accepted: 16 April 2021

Published: 18 April 2021

Publisher's Note: MDPI stays neutral with regard to jurisdictional claims in published maps and institutional affiliations.



Copyright: © 2021 by the authors. Licensee MDPI, Basel, Switzerland. This article is an open access article distributed under the terms and conditions of the Creative Commons Attribution (CC BY) license (<https://creativecommons.org/licenses/by/4.0/>).

1. Introduction

Separation processes in the oil, gas and chemical industries account for up to 15% of their total energy requirements [1–4]. Light hydrocarbons (C_1 – C_9) are vital chemical feedstocks and energy resources around the world [5]. In addition, olefin separations are critical for the chemical industry, with the greatest demand on high purity propylene (C_3H_6). The demand for high purity propylene has risen sharply in recent years, and the compound is now the second most widely produced hydrocarbon by volume in the world after ethylene [3,6–9]. In 2019, the production of propylene was around 145 million tons globally [5]. Propylene is an intermediate essential chemical in a large number of important chemical industries such as polypropylene based plastics, propylene oxides, isopropanol, acrylonitrile, and other copolymers [3,6,9–19]. Steam/catalytic cracking of higher chain hydrocarbons is the main method of producing propylene, although the resulting product inevitably contains amounts of propyne. Propyne (C_3H_4) is a common impurity that is known to cause a poisoning effect of the catalyst during the cracking process, with detrimental effect on the production of propylene [3]. To meet polymer grade propylene requirements, the content of propyne must be reduced to less than 5 ppm. It is therefore imperative to remove propyne from the propylene gas streams to produce the required propylene polymer grade gas (>99.99% purity). The separation of propane (C_3H_8)

and propylene is well reported in literature given its demanding energy requirements and the close relative volatilities of both compounds at the temperature range of operation (typically between 244–327 K) [2,7–10,13,14,17]. However, only a few studies have reported the separation of C₃H₄/C₃H₆ mixtures [4,20–22]. This separation is very challenging due to the physical and chemical similarities (molecular size C₃H₄: 4.16 × 4.01 × 6.51 Å [3] and C₃H₆: 5.25 × 4.16 × 6.44 Å [3]) between propyne and propylene compounds; more so than C₂H₂/C₂H₄ separations, for example [4]. Cryogenic distillation is the most commonly used method. Typically, it requires more than 100 theoretical stages to perform the separations of the gas fractions under low temperature and high pressure conditions [6], resulting in very high energy demands. Other technologies involve adsorption-based separations using a variety of materials such as zeolites and carbons in a variety of settings such as pressure, vacuum, or temperature swing settings [2,7,12,14,23–26]. Low separations and selectivity remain a challenge in difficult separations like those related to propyne and C₃H₆ separations. New developments in metal organic frameworks (MOFs) and the development of crystal engineering represent huge potential for previously difficult separations [27–29]. Metal organic frameworks, sometimes called metal coordinated polymers, are crystalline micropore materials with huge potential, owing to the flexibility in their chemical structure and intrinsic properties that can be fine-tuned to suit a given gas separation application [30–32]. Accordingly, the MOF internal aperture can be tuned for selective size or shape separation. They generally comprise organic ligands and inorganic metal clusters. Accordingly, the changes in structure pore size, one of the most appealing features of MOFs, and functional groups lends itself to many gas applications and separation processes. The structural flexibility and dynamic behavior of metal organic frameworks, such as the gate-opening effect due to variations in temperature, pressure, or other external stimuli, are another distinct feature of metal organic frameworks compared to traditional adsorbents such as zeolites [5]. A class of MOFs (hybrid ultra-microporous materials) are setting a new benchmark in a number of gas separations [27]. These materials are based on 3D Zn/Cu/Ni coordination networks that contain metal nodes in addition to organic linkers. Anions such as SiF₆²⁻ (SIFSIX), NbOF₅²⁻ (NbOFFIVE) form bridges in the MOF structure and are reported to have potential application in gas separations, such as C₃H₆/C₃H₈ and other lower alkene/alkane separations.

Gas hydrocarbons are adsorbed inside the molecule and held via van der Waals, metal-binding or hydrogen interactions, depending on the type of MOF used. To this end, equilibrium, kinetic, or molecular sieving separations can be the predominant mechanism that aids the use of a particular MOF in a given gas separation. Molecular sieving is based on size/shape exclusion, while thermodynamic equilibrium separation depends on the type and strength of the interactions and the affinity of the host-guest interactions i.e., MOF and the gas species. In equilibrium separations, there are relative thermodynamic affinities between the gas species and the MOF adsorbent via the introduction of strong interaction sites on the MOF frame. Lewis acidity related to an uncoordinated open metal site MOF is used in CO₂ or olefin separations. These interactions form strong bonds which is the major challenge associated with their use in such separations due to the associated extra energy requirements related to the desorption of the gas and its subsequent release and separation, in addition to the MOF regeneration. Kinetic operations are based on the diffusivity of the gas compounds and their relative selectivity.

The use of metal organic frameworks for the separation of propyne/propylene is still in the early stages, with few reported studies in literature [4]. The first study on C₃H₄/C₃H₆ separation was reported using [Cu(4,4'-bipyridine)(trifluoromethanesulfonate (OTF)⁻)₂](ELM-12) [21]. This material showed good potential for adsorption selectivity through the estimation of the ideal adsorbed solution theory (IAST) selectivity at a trace concentration of propyne (ratio 1/99 C₃H₄/C₃H₆), with good adsorption capacity at low-pressure range. The work highlighted the potential of metal organic frameworks of flexible structures for hydrocarbon separation at low concentrations. Anion pillared metal organic frameworks with various structures were also studied, including the NbOF₅²⁻ and SiF₆²⁻

pyrazine based MOF family (NbOFFIVE-1-Ni (sometimes called KAUST-7 [33]), SIFSIX-2-Cu, SIFSIX-3-Ni, SIFSIX-3-Zn) [18]. The study highlighted that the geometric disposition and pore size of SiF_6^{2-} anions could be varied to best match the propyne molecules, resulting in very promising separation under the applied experimental conditions. The adsorption capacity reportedly reached 2.6 mmol g^{-1} for propyne concentrations of around 300 ppm. The study reported that both molecules were adsorbed, limiting productivity in separation [5]. Li et al. [4] screened 20 different MOF materials with varying structures, pore sizes, preparation methods, and functional groups for propyne/propylene separation. Their study showed that one material, called UTSA-200, exhibited great potential ($95 \text{ cm}^3 \text{ cm}^{-3}$ at low pressure and 298 K) at an ultralow concentration (0.1:99.9 *v/v* $\text{C}_3\text{H}_4/\text{C}_3\text{H}_6$). The high affinity was reported to be related to the suitable pore size resulting from the rotation of the pyridine rings in the MOF with blocking propylene effect [4,5]. Recently, calcium based metal organic frameworks were investigated for $\text{C}_3\text{H}_4/\text{C}_3\text{H}_6$ separation [3]. An uptake gas value of 2.4 mmol g^{-1} was recorded at low pressures and trace concentrations.

In the few reported studies on propyne/propylene separation, very low concentrations were studied at pressures up to 1 bar. To establish a good trade off, high productivity and purity is required from the adsorbent material. In addition, most studies considered the adsorption capacity alone, while a few considered breakthrough analysis for a number of different cycles. There is a lack of systematic studies on this particular separation that take into account the adsorption isotherms and kinetics of the stream under consideration. Targeting materials with well-developed porous structures and stability is required to enhance the separation of propyne and propylene, to ensure the high purity of propylene, which is needed for industrial grade applications, and to reduce the energy requirements of this process. As mentioned earlier, the study of the selectivity is important to establish the type of integration between the gas and the MOF adsorbent to facilitate the understanding of the desorption and the reversibility of the interaction. Accordingly, in this study, a systematic approach was considered to study the effect of two types of pyrazine-based inorganic anions (SiF_6^{2-} , NbOF_5^{2-}) metal organic frameworks (SIFSIX-3-Ni and NbOFFIVE-1-Ni) under a range of temperatures (300–360 K) and pressures (up to 100 kPa) for the separation of propyne/propylene in various concentrations (10/90 *v/v*). Adsorption capacities were analyzed using four isotherm models, i.e., single (Langmuir and Freundlich) and multi constant isotherms (Sips and Toth). No other reported studies have addressed the mathematical isotherm fitting of the experimental data for the $\text{C}_3\text{H}_4/\text{C}_3\text{H}_6$ system in combination with the metal organic frameworks used in this study. Such data are important in engineering calculations related to scale up and industrial applications. In addition, the selectivity was analyzed using the ideal adsorbed solution theory (IAST). Dynamic studies were conducted and breakthrough curves were established at varying numbers of cycles.

2. Experimental Materials and Methods

High purity analytical materials were supplied by Sigma-Aldrich and Buzwair Inc. Qatar. Chemical structures and characteristics of propyne and C_3H_6 are shown in Table 1. Gases were of 99.99% purity.

Table 1. Characteristic information for adsorbents and adsorbate gases.

Sorbent	BET ($\text{m}^2 \text{g}^{-1}$)	Pore Size (nm)	Pore Volume ($\text{cm}^3 \text{g}^{-1}$)	Ref	Size (\AA^3) *	References
NbOFFIVE-1-Ni	248	0.139	0.095	This study, ref. [34]	D1:4.66, D2:3.21, D3:4.9 D2:3.047	[1,18] [1]
SIFSIX-3-Ni	368	0.36	0.167	This study, ref. [34]	D1:5.03, D2:3.75, D3:4.6 D2:4.2 D1:5.047	[18] [4] [1]
Hydrocarbon	Structure				Size (\AA^3) *	References
C_3H_4					$4.16 \times 4.01 \times 6.51$	[3–18]
C_3H_6					$5.25 \times 4.16 \times 6.44$	[3–5,18]

* D1, D2 and D3 refer to distances as illustrated in Figure 1b.

2.1. Adsorbent Synthesis

The two metal organic frameworks (NbOFFIVE-1-Ni and SIFSIX-3-Ni) were prepared as detailed in our earlier work [34]. Both metal organic frameworks were pyrazine based, as detailed in Figure 1. The metal organic frameworks were architected by the bridging of the pyrazine- Ni^{2+} square grid layers with NbO_5^{2-} (Figure 1). The difference between the NbO_5^{2-} and SiF_6^{2-} resulted in pyrazine moieties free rotation, and it affected the pore cavity which is smaller in NbO_5^{2-} compared to that of SiF_6^{2-} (= hexafluorosilicate) (Table 1).

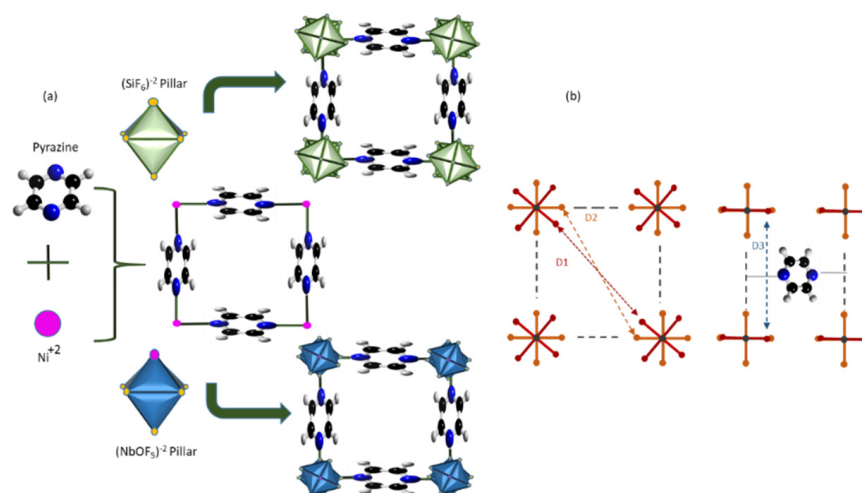


Figure 1. (a) Schematic of the basic structure of the pyrazine based metal organic frameworks used in the study. (b) Structural representation of the metal organic frameworks and size dimensions. Values of D1, D2 and D3 are given in Table 1 (dimensions are not to scale and for illustration purposes).

2.2. Sample Characterization:

2.2.1. Brunauer-Emmett-Teller (BET) Analysis

Liquid nitrogen was used for the N_2 gas adsorption tests at 77 K. Micromeritics characterization was carried out using ASAP 2420 surface and porosity analyzer (Micromeritics GmbH, Unterschleißheim, Germany). Surface area was established using BET model while pore size distribution was found using the BBJ method [34]. Table 1 presents the main characteristics of the metal organic frameworks used.

2.2.2. Thermogravimetric Analysis (TGA), SEM and FTIR

TGA analysis may be used to establish the weight loss of metal organic frameworks under thermal stress with high temperatures as an indication to the sample thermal stability. Tests were conducted using a Perkin Elmer Pyris 6 analyzer. Details of these tests have been reported by Khraisheh et al. [34].

Furthermore, Fourier-transform infrared spectroscopy (FTIR) (using Bruker Vertex 80) for the adsorbents was conducted in the range of 4000–400 cm^{-1} . In addition, SEM analyses were conducted following standard protocols.

2.3. Gas Uptake

Equilibrium and Kinetic Breakthrough Gas Adsorption Studies

To establish the maximum and equilibrium uptake capacity of the solids towards $\text{C}_3\text{H}_4/\text{C}_3\text{H}_6$ gases, Micromeritics ASAP 2420 (Germany) was used. Samples of around 100 mg were outgassed for at least 12 h under vacuum at 338 K before the adsorption/desorption experiments. Tests were conducted at a range of temperatures between 300–360 K (controlled via water (300–320 K) or oil (340–360 K) jacket) and pressures from 0–100 kPa. An in-house simple setup was used to test the breakthrough experiments (dynamic tests). The setup consisted mainly of a small quartz adsorption column (I.D 4 mm, height: 160 mm), gas flow controllers and gas analyzer. The required amount of adsorbent was used in the columns and then activated inside the column at 338 K for a couple of hours using helium (He) gas to ensure that any unwanted inert gases had been fully purged from the column. To eliminate any errors in the use of the gas mixtures, a (10/90 *v/v*) $\text{C}_3\text{H}_4/\text{C}_3\text{H}_6$ gas mixture cylinder was purchased (Buzwair gas Inc. Qatar) and used in the experiments. A total flow rate of 5 mL (STP min^{-1}) was used in all experiments. The flow rate was found to offer the best optimum conditions without having to fluidize the bed. The beds were regenerated ahead of a new gas breakthrough cycle using He (99.99 purity) for 30 min at 298 K and a flow rate of 5 mL min^{-1} . The same sample of solid MOF sorbent was used for up to eight successive breakthrough cycles in order to study the stability of the adsorbent during multiple cycle operations of sorption and desorption. The experimental procedure for each cycle was identical to that described above.

3. Theoretical Modeling

3.1. Isotherm and Kinetic Models

The adsorption isotherms of the pure compounds on the NbOFFOVE-1-Ni, SIFSIX-3-Ni were determined. Many models are reported in the literature to describe the adsorbent capacity for a certain species. The most commonly used in the case of gas-solid adsorption system are Langmuir, Freundlich, Sips and Toth isotherms [10]. The first two are known as the two parameter models, while the latter models are a hybrid combination of the two parameter models.

The Langmuir model is one of the most widely used isotherms in many applications including solid-gas and solid-liquid separations. The model is based on the assumption of monolayer interaction between the adsorbent and adsorbate with the assumption that all adsorption sites have similar adsorption energy requirements. Equation (1) represents one of the simplest forms to describe the Langmuir isotherm, where the maximum or saturation adsorption capacity is related to the system pressure and Langmuir constant, as shown in Equation (1):

$$Q = q_{\text{sat}} \frac{k_1 P}{1 + k_1 P} \quad (1)$$

where Q (mmol g^{-1}) is the adsorption capacity, q_{sat} (mmol g^{-1}) is the equilibrium uptake capacity of the gas species, P is the system pressure (kPa), and k_1 : isotherm constant related to the energy of adsorption

The two main factors of Equation (1) were estimated from experimental data and used to establish the model fit of the data to the isotherm. The applicability of the isotherm is

typically related to another factor that is associated with the Langmuir model, as described in Equation (2):

$$R_l = \frac{1}{1 + k_l P} \quad (2)$$

The value of the separation factor R_l is indicative of the ability of the model to fit the experimental data.

The Freundlich isotherm, on the other hand, is based on the assumption of multilayer adsorption with various adsorption energies [35]. In this model (Equation (3)), the increase in the pressure of the system increases the uptake capacity of the adsorbent.

$$Q = k_f P^{\frac{1}{n}} \quad (3)$$

where k_f is the Freundlich constant and n is a constant. A value of n lower than 1 is indicative of chemisorption rather than physisorption.

Although both models are widely used in many applications, their ability to fit the experimental data in a wide range of applications is limited in systems related to adsorption of many hydrocarbons. Accordingly, hybrid multiconstant models that are based on the two models have been used with better representation of the adsorption of hydrocarbons on solid materials.

The Sips model is an isotherm derived from both Langmuir and Freundlich isotherms and is presented in Equation (4) [10]:

$$Q = q_{\text{sat}} (k_s P)^{1/m} / (1 + k_s P)^{1/m} \quad (4)$$

where k_s is Sips constant and m is a constant that represents deviation from ideal heterogeneity of the adsorption system and is typically considered as intensity factor with values above 1 indicative of a heterogeneous adsorption. Equation (4) reduces to its Langmuir form (Equation (1)) in cases when m equals unity. The Sips model is known to be best applied in cases where the system operates at higher-pressure conditions. The Toth isotherm [36] (Equation (5)), on the other hand, is another hybrid combination of the Langmuir and Freundlich isotherm that is reported to have better data fitting in applications at a wider variety of pressures compared to the Sips model.

$$Q = q_{\text{sat}} \left\{ \left(\frac{(k_t P)^n}{(1 + k_t P)^n} \right) \right\}^{\frac{1}{n}} \quad (5)$$

where k_t and n are Toth constants specific for adsorbate-adsorbent pairs, while n indicates the affinity of the adsorption. A value of n close to 1 is an indication of the system heterogeneity. As with the Sips model, a value of 1 reduced the Toth equation back into Langmuir isotherm. The applicability of this model in a good range of system pressure application resulted in its wider application in gas solid adsorption systems.

Statistical analyses were used to evaluate the fit of the experimental data to the various models. The most reported parameter used is based on the average absolute relative deviation (AARD), coefficient of determination (R^2) (Equations (6) and (7), respectively).

$$\text{AARD}(100\%) = \frac{100}{N} \sum_{i=1}^N \left| \frac{Q_{\text{exp}} - Q_{\text{pred}}}{Q_{\text{exp}}} \right| \quad (6)$$

$$R^2 = 1 - \frac{\sum_{i=1}^N (Q_{\text{pred}} - Q_{\text{exp},i})^2}{\sum_{i=1}^N (Q_{\text{pred}-i} - \bar{Q}_{\text{exp}})^2} \quad (7)$$

where Q_{pred} is the predicted amounts, Q_{exp} is the values of Q obtained experimentally, and N is the number of the experimental data points used in the isotherm fit.

3.2. Isothermic Heats of Adsorption, IAST Selectivity and Adsorption Kinetics

The isosteric heat of adsorption makes it possible to characterize the surface properties of adsorbents, catalysts, and other materials, and provides information on the homogeneity and heterogeneity of surface. The calculation of the isosteric heats of adsorption (Q_{st} (kJ mol^{-1})) is essential for an understanding of the strength of the interactions between the solid surface and the adsorbate in addition to any energetic heterogeneity in the solid surface. The calculations are typically based on the fundamental Clausius-Clapeyron equation:

$$Q_{st} = RT^2 \left(\frac{\partial \ln P}{\partial T} \right)_{q_{sat}} \quad (8)$$

where P and T are the system pressure and temperatures and q_{sat} is the saturated equilibrium uptake amount (mmol g^{-1}).

To assess the selectivity and feasibility of the separation, the IAST selectivity was considered for $\text{C}_3\text{H}_4/\text{C}_3\text{H}_6$ gases on the two metal organic frameworks employed in this study. The IAST calculations facilitate the study of the selectivity in binary gas mixtures. A full mathematical description is available elsewhere [6,10,37,38].

Adsorption kinetics is fundamental for engineering evaluation of adsorption systems. Typically, models derived from Fick's law of micropore diffusion are employed to model adsorption uptake curves via the calculation of the intercrystalline diffusivity (D_c) [10]. An analytical solution of the equation based on the assumption of approximate cylindrical geometry of the solids is given as:

$$\frac{q}{q_\infty} = 1 - \sum_{n=1}^{\infty} \frac{4\alpha(1+\alpha)}{4 + 4\alpha + \alpha^2\beta_n^2} \exp\left(-\frac{D_c}{r_c^2} \beta_n^2 t\right) \quad (9)$$

where q_∞ is the equilibrium adsorbed amount (mmol g^{-1}), t is the time (s), and constants α and β are calculated as detailed in [10].

4. Results and Discussion

4.1. Adsorbent Characterization

The SIFSIX and NbOFFIVE metal organic frameworks were synthesized and characterized as described in our earlier work [34]. Figure 2 offers some of the main characteristics obtained, including SEM, FTIR, N_2 adsorption desorption, and TGA analysis. In addition, Table 1 presents the estimated surface area and pore volumes. Thermal stability is essential for proper application of microporous materials in separation processes. The stability of the prepared materials was tested in a harsh temperature environment, i.e., up to 750°C , by thermogravimetric analysis in the presence of nitrogen gas. The TGA isotherms are given in Figure 2i for both sorbents and represent the change in the weight of the material at elevated temperatures. A steep change in the mass of the adsorbent indicates a less stable structure and the possibility of material deterioration at higher temperature settings. At $280\text{--}300^\circ\text{C}$, both materials underwent between 10–15% decrease in mass. The decrease was much steeper in the case of SIFSIX compared to NbOFFIVE at temperatures above 300°C . The results of TGA obtained in our study were in good agreement with those reported in Bhatt [39] and Kumar [40]. The initial loss of mass is usually due to the evaporation of free water and other volatile compounds. A large drop in mass at elevated temperatures, as is the case in SIFSIX, may result in the decomposition of the material and the loss of wall and structural integrity [30,35]. The interactions between the different functional groups in a material can clarify the gas uptake. FTIR spectroscopy (Figure 2ii) was recorded in the range of $400\text{--}4000\text{ cm}^{-1}$. For NbOFFIVE-1-Ni, the peaks at 3221, 1615, 1402, and 465 cm^{-1} most likely correspond to the characteristic nickel O–H stretching. A SEM micrographs for the two prepared materials (Figure 2iv) showed multisized agglomerations in both materials with the pore size in the range of 100–600 nm. Voids are clearly present between the uniform particles. The porous nature of the materials was tested using N_2 adsorption.

A significant difference in pore size and volume (Figure 2iii) was found between the SIFSIX and NbOFFIVE; both were higher for SIFSIX. The pore size for this compound was nearly 2.6 times higher than that recorded for the Nb MOF (Table 1), indicating a more enhanced surface area and porosity, and the formation of a well-defined structure [17]. The shape of the adsorption and desorption isotherms (depicted in Figure 2iii) clearly indicated a reversible Type-I isotherm in accordance with IUPAC categorization. This type indicated the formation of uniform narrow mesopores and a wider distribution of the pores [10,36,41]. The initial steep rise in the N₂ adsorption–desorption isotherm at a low relative pressure (P/P_0 less than 0.001) is typically associated with the formation of microporosity. The high-adsorbed volume values (Figure 2iii) at relative pressures higher than 0.8 have been attributed to the N₂ capillary condensation in the antiparticle pores, and may indicate expandable pores and a flexible structure which may lead to what is known as gate-opening effect [35]. The N₂ adsorption–desorption isotherms did not indicate the presence of a clear hysteresis loop at low P/P_0 ratio. A slight hysteresis effect was present at higher P/P_0 ratio.

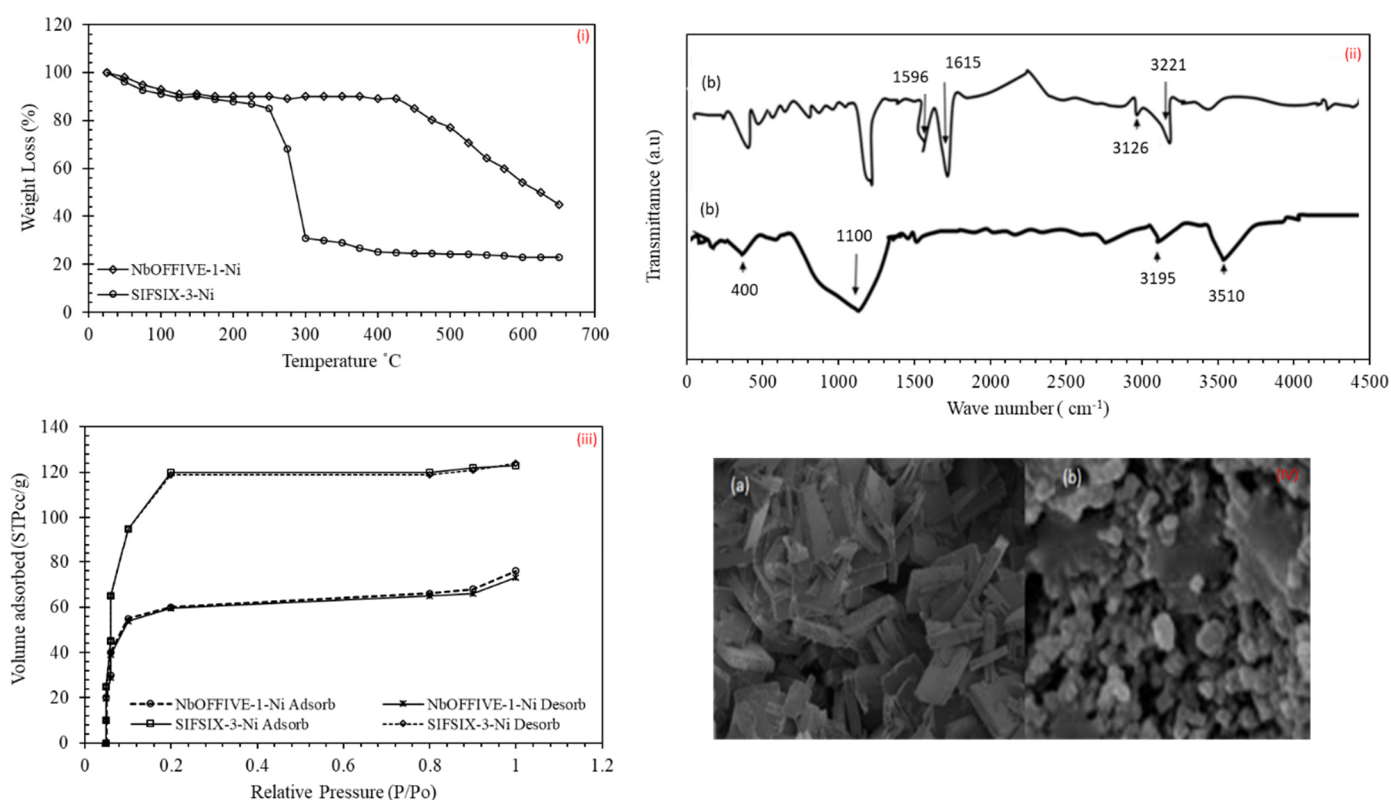


Figure 2. Characterization results for SIFSIX-3-Ni and NbOFFIVE-1-Ni; (i) TGA; (ii) FTIR; (iii) N₂ adsorption/desorption; (iv) SEM images (a) NbOFFIVE-1-Ni, (b) SIFSIX-3-Ni.

It has been reported that the separation of C₃H₆/C₃H₈, for example, is dominated by size selection separation [1]. It is hence expected that the separation of C₃H₄/C₃H₆ will follow a similar mechanism as in both cases of fluorinated metal organic frameworks (NbOFFIVE and SIFSIX were deployed under similar experimental conditions). The restrictive pore size of the metal organic frameworks due to the prevention of the pyrazine moieties (Figure 1) affects the size selection between gas species. From the N₂ adsorption data, BET areas were estimated to be 248 and 368 m² g^{−1} for NbOFFIVE and SIFSIX, respectively (Table 1). The experimentally obtained total pore volumes were 0.095 and 0.167 cm³ g^{−1} for NbOFFIVE and SIFSIX, respectively.

4.2. C_3H_4/C_3H_6 Uptake and Separation

The potential of using the microporous metal organic frameworks for the selective adsorption–desorption and molecular interactions and binding nature of propyne over propylene at low pressure ranges (up to 100 kPa) and various temperatures was investigated. The results are presented in Figures 3 and 4. Figure 3a,b depicts an example of adsorption and desorption gas uptake for both adsorbents at a range of pressures up to 100 kPa. The figure shows the adsorption at 300 K as an example. Similar trends were obtained at different temperatures. The figure clearly reveals that different uptake values can be obtained in the case of propyne and propylene, indicating an effective separation due to the differences in the uptake values and steepness of the isotherms obtained. Both figures clearly show that propyne is adsorbed in a larger amount at a given pressure in comparison to propylene. A maximum uptake value of 3.28 and 2.99 mmol g^{-1} was obtained for propyne on SIFSIX-3-Ni and NbOFFIVE, respectively at 300 K. The maximum absorbed values for propyne were lower than those for propyne on both adsorbents, as can be seen from Figure 3a,b. Values of 2.9 and 2.39 mmol g^{-1} were obtained for propylene on SIFSIX and NbOFFIVE, respectively. The C_3H_6 and C_3H_4 values on the SIFSIX were higher than those recorded for the NbOFFIVE-1-Ni for the entire pressure range at a given temperature. It is also evident that the difference in the adsorption of C_3H_4 and C_3H_6 on SIFSIX was wider (Figure 3a) than that obtained on the NbOFFIVE MOF (Figure 3b). This indicated that the separation of propyne from C_3H_6 on the SIFSIX was more effective than that on the NbOFFIVE based MOF, and provides evidence of the potential for C_3H_4/C_3H_6 separation applications. A value of 2.85 mmol g^{-1} was reported for SIFSIX-3-Ni at 298 K for propylene [42]. The anion pillar NbOF_5^{2-} is bulkier than SiF_6^{2-} and has longer F-Nb bond length (1.89 compared to 1.68 Å for SIFSIX), resulting in a thinner and longer pore space (4.66×7.88) which leads to lower propyne capacity [18]. This led us to conclude that small changes to the pore structure can have a major influence on the selectivity and absorbability of the adsorbate on the selected MOFs.

In addition, study of the adsorption–desorption behavior for propyne and propylene for both adsorbents (Figure 3) was important to establish the reversibility (regeneration ability) for the adsorbents. It is clear that both adsorbent isotherms show reversibility upon uptake of propyne and C_3H_6 gases. It is also evident that the hysteresis effect is more pronounced in propyne adsorption for both sorbents compared to that for C_3H_6 . This indicated a strong affinity and molecular interactions between C_3H_4 molecules and the structure of the sorbents. A less defined hysteresis effect is realized in the case of propylene adsorption on both solids. A similar effect was reported in a recent study by Lin et al. [42]. Li et al. [4] reported that some metal organic frameworks such as SIFSIX-1-Cu, SIFSIX-2-Cu-i, ELM-12 have a strong interaction with C_3H_4 at pressures less than 20 kPa. These interactions were exhibited in a steep adsorption uptake isotherm at a fixed temperature over propylene with the reported benchmark uptake values [4]. One issue related to the aforementioned materials is that their pore sizes were large, allowing the passage of both gases, and hence reducing their potential selectivity.

The effect of temperature on the adsorption of C_3H_4 and C_3H_6 on both MOFs is given in Figure 4. Temperatures in the range of 300–360 K were used for pressures up to 1 kPa. It can be seen from Figure 4a–c that the temperature has a profound impact on the removal and uptake rate for all adsorbents. It is clearly shown that the uptake of the gases is lowered by the elevation in temperature. Other adsorption systems such as C_3H_6 and C_3H_8 , as reported in studies, showed similar trends with respect to uptake values vs. temperature [10]. No other studies have shown the full experimental isotherm results for propyne and C_3H_6 systems. In all cases, the adsorption of C_3H_4 is higher than that for propylene at all temperature ranges and in both adsorbents. In addition, SIFSIX outperformed NbOFFIVE for the selectivity of C_3H_4 . It can also be noted that a steep increase in the adsorption capacity at the lower pressure range is more apparent in the case of C_3H_4 and SIFSIX combination at all temperature ranges in comparison with the other adsorbent/adsorbate systems (Figure 4a). A similar result was reported, but

in the C_3H_6 and C_3H_8 systems on different metal organic frameworks [10]. To facilitate a good comparison, Figure 4c also shows experimental uptake isotherms at a selected temperature for both adsorbents and adsorbate systems. The superior uptake capacity of SIFSIX for propyne is evident, especially at low-pressure ranges (<20 kPa), indicating a strong interaction between the SIFSIX and C_3H_4 . Comparisons between the uptake capacity and those published in the literature are presented in Table 2. This higher affinity and uptake values may also be related to the better BET surface area and pore structure of the SIFSIX compared to NbOFFIVE metal organic frameworks (Table 1). Figure 4c shows that the gap between the two isotherms for C_3H_4 and C_3H_6 are larger in SIFSIX compared to that in NbOFFIVE. A marked gap means that the separation is feasible for this system, and will be further studied via IAST analysis. The kinetic diameter of the molecule will have a major effect on the selectivity of one gas over another. Propyne is a linear molecule ($4.16 \times 4.01 \times 6.51$ Å), while C_3H_6 is a larger molecule which is typically curve-shaped with $4.64 \times 4.16 \times 6.44$ Å [4]. Irrespective of the linear shape, the existence of the methyl group in both gases makes their kinetic diameters quite close (4.2 and 4.6 Å for C_3H_4 and C_3H_6 , respectively). This small difference is one of the main reasons for the difficulty and energy intensity of their separation. SIFSIX and NbOFFIVE have a range of reported dimensions, depending on methods of preparation, post-treatment and experimental conditions, (Table 1), which clearly indicates that SIFSIX is more suited for the adsorption of C_3H_4 from C_3H_6 . A micropore analysis of the SIFSIX and kinetic diameter (average 4.2) will allow both C_3H_4 and C_3H_6 to enter the pores. Nonetheless, it seems that a large number of anions (SiF_6^{2-}) in the pores and channels of the framework [4] provides a better binding ability for alkynes, as compared to alkenes, creating a preferred sieving effect towards propyne. This results in the excellent selectivity and separation ability of SIFSIX compared to NbOFFIVE. The maximum equilibrium adsorption value reported here for the SIFSIX MOF was higher than that reported for the same material and C_3H_4 separation (1.87 mmol g^{-1}) [4]. The difference may be attributed to the different $v/v\%$ ratios used in the reported study. In addition, the value recorded in our work is similar to the benchmark uptake value reported for UTSA-200 ($[Cu(azpy)_2(SiF_6)]_n$; azpy = 4,4'-azopyridine) in a recent work by Li et al. (4). The main reason for the good reported selectivity is the small aperture size of the UTSA-200 (3.4 Å), meaning that size exclusion is the only dominating mechanism in this case, compared to stronger interactions between SIFSIX and the C_3H_4 gas. Yang et al. [18] reported that the precise tuning of the size of the inorganic anion hybrid ultramicroporous materials based on SiF_6^{2-} and $NbOF_5^{2-}$ serves as a single molecule trap for propyne.

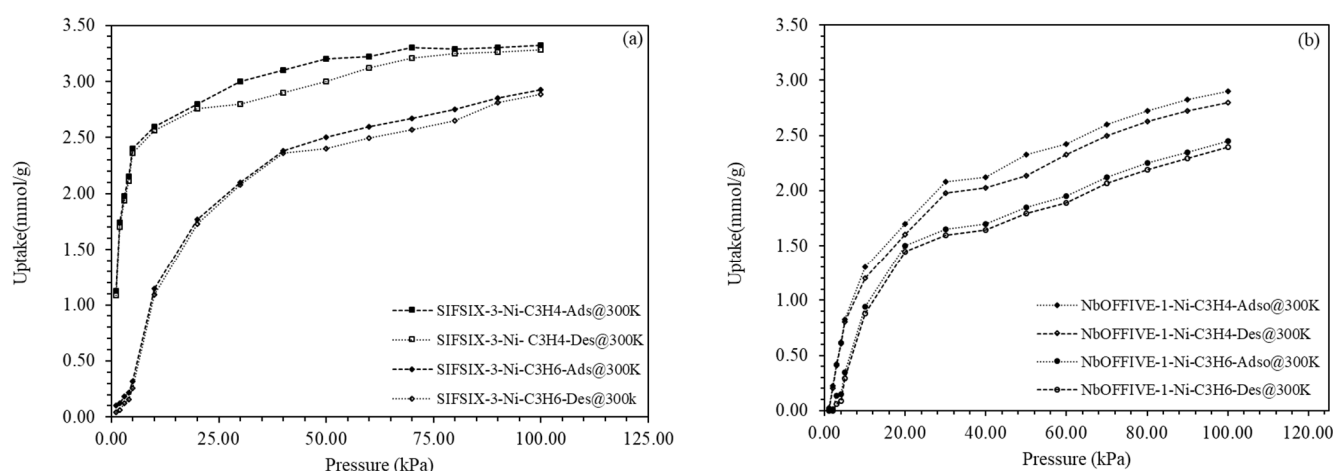


Figure 3. (a) adsorption/ desorption of C_3H_4 on SIFSIX-3-Ni at 300 K and (b) adsorption/ desorption of C_3H_6 on NbOFFIVE-1-Ni at 300 K.

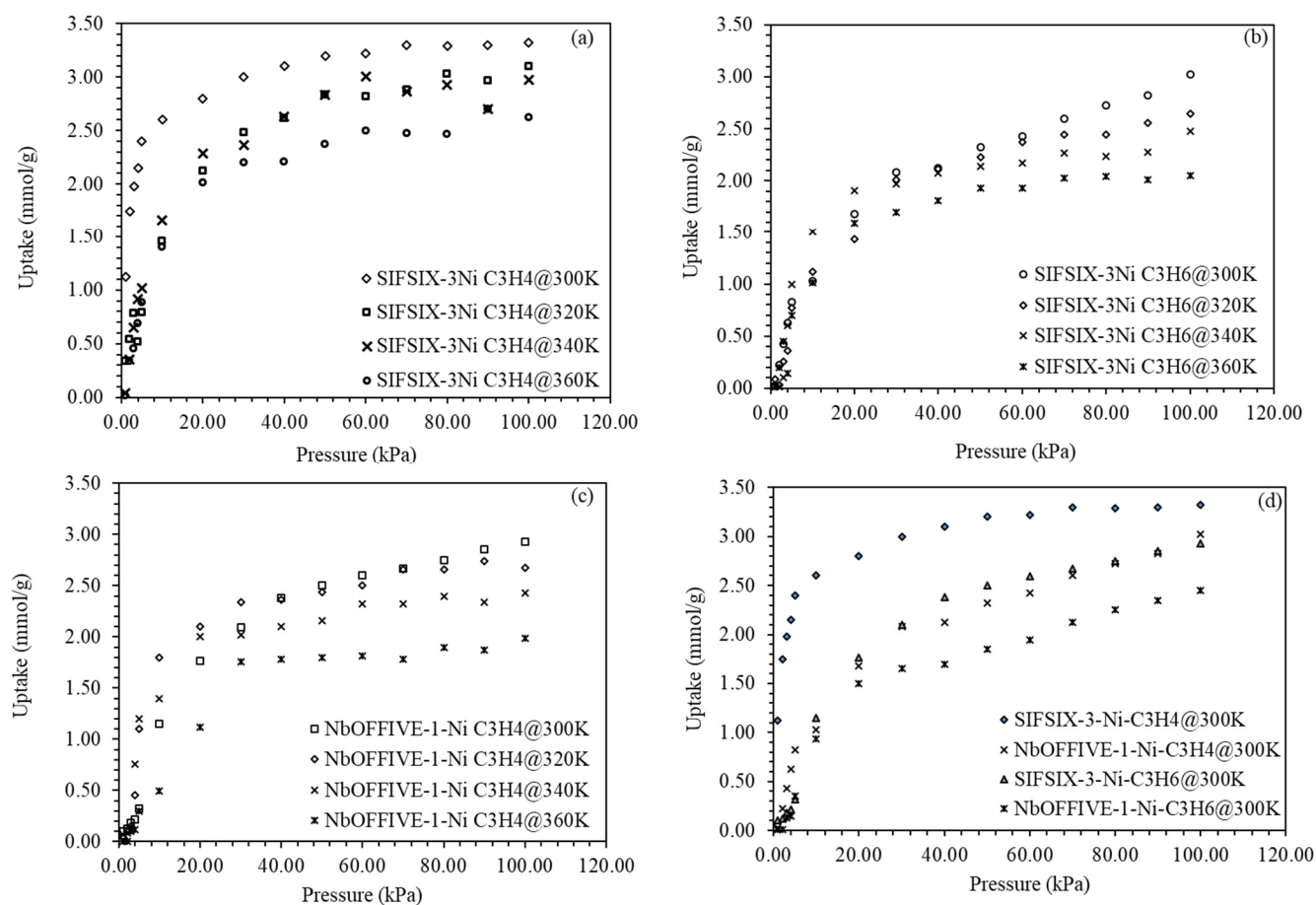


Figure 4. Full experimental isotherms at different temperatures (300–360 K) (a) C₃H₄ and SIFSIX-3-Ni (b) C₃H₆ and SIFSIX-3-Ni (c) C₃H₄ and NBOFFIVE-1-Ni (d) C₃H₆ and NBOFFIVE-1-Ni.

Table 2. Uptake adsorption values reported in the literature.

Material	Adsorption Uptake (mmol g ⁻¹)	Ref.
C ₃ H ₄ from C ₃ H ₄ /C ₃ H ₆		
SIFSIX-3-Ni	3.2	This study
NBOFFIVE-1-Ni	2.9	This study
SIF-Six-2-Cu-i	1.73	[3]
SIFSIX-3-Ni	2.7	[3]
SIFSIX-1-Cu	0.19	[18]
SIFSIX-2-Cu-i	0.2	[18]
SIFSIX-3-Ni	2.65	[18]
[Cu(dhbc) ₂ (4,4'-bipy)]	0.25	[43]
NK-MOF-Ni	1.83	[3]
NK-MOF-Cu	1.76	[3]

4.3. IAST Selectivity and Isothermic Heats of Adsorption

Figure 5a shows the isosteric heats of sorption (Q_{st}) as a function of uptake amounts of propyne and propylene. The trends in Figure 5a clearly indicate that the Q_{st} of C₃H₄ is higher than that for C₃H₆ for both SIFSIX and NBOFFIVE metal organic frameworks. A higher Q_{st} value is indicative of strong affinity and interactions between the solid pore structure and the gas being adsorbed. At zero uptake, the maximum value of Q_{st} is attained.

For SIFSIX and C_3H_4 system, the Q_{st} zero was around 45 kJ Kmol^{-1} and for propylene system, the maximum value was around 30 kJ Kmol^{-1} . Similar trend was observed in the case of NbOFFIVE with the gas systems where isosteric heats of adsorption at zero uptakes were 38 and 30 kJ Kmol^{-1} , respectively, for propyne and propylene systems. In both cases, the values of Q_{st} at zero coverage were higher for C_3H_4 than for C_3H_6 , indicating a stronger affinity and interactions between the C_3H_4 molecules and the MOF structures. In addition, the value for propyne for the SIFSIX is higher than that obtained for NbOFFIVE, also indicating the stronger affiliation and intermolecular interactions between the SIF and propyne gas. In addition, the general trend for all cases is that Q_{st} decreases gradually with the increase in uptake rate of the gases on the pore structure of the solids. The continuous decrease at a similar rate indicates the homogeneity of the pore environment. Typically, as Q_{st} increases with higher uptake rates, heterogeneity of the surface is usually present [10]. In addition, the differences between the propyne and propylene for both solids is a good indication of the separation possibilities of the two gases.

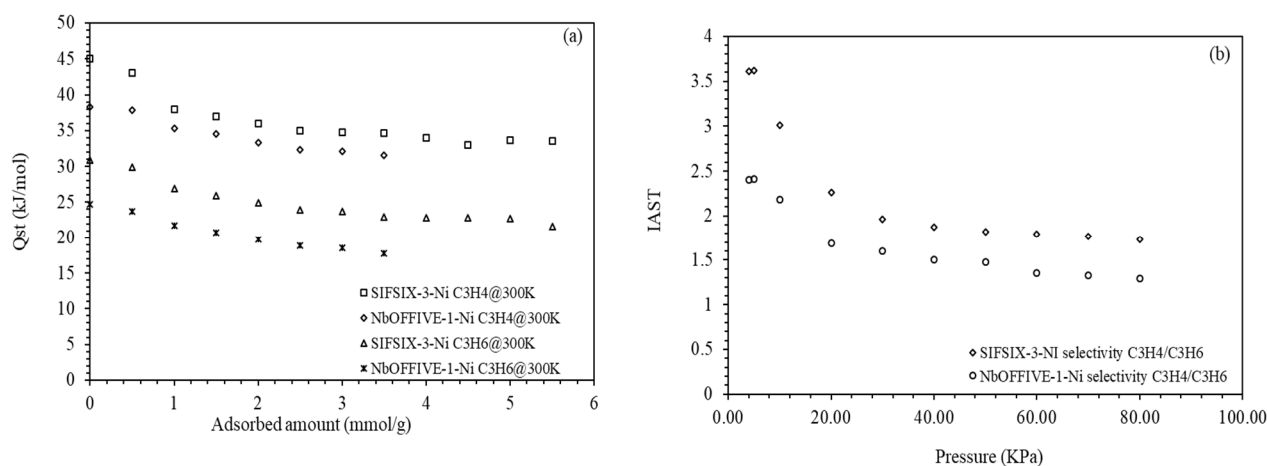


Figure 5. (a) Isosteric heats of sorption for SIFSIX and NbOFFIVE metal organic frameworks for both C_3H_4 and C_3H_6 as a function of adsorption uptake, (b) IAST selectivity for C_3H_4/C_3H_6 system on both adsorbents at 300 K.

To assess the separation ability of the two compounds, the selectivity (a key factor and application index for industry) of the ideal adsorbed solution theory (IAST) were calculated and are presented in Figure 5b for 10/90 v/v binary gas mixtures of C_3H_4 and C_3H_6 at 300 K. The IAST is typically employed, as the isotherms for binary systems of gases are difficult to measure. In the IAST estimations, it was assumed that the gas species had formed an ideal mixture. This approximation has been used in many studies of metal organic frameworks and different gas species. Full details on the and mathematical treatment of Raoult's law are given elsewhere [10]. As indicated in Figure 5b, the selectivity of propyne over propylene for both metal organic frameworks was higher at lower pressure operations compared to pressures above 20 kPa. In some studies using different flexible structures, metal organic framework trends for propane/propylene adsorption, for example, showed higher selectivity at pressures above 60 kPa, indicating increased adsorption due to the "gate opening" effect of the MOF structures used [10]. The trend observed in this investigation led us to the conclusion that the structure of the used metal organic frameworks did not change with an increase of pressure in the range used in this study. In addition, the SIFSIX showed a higher selectivity between the two gases compared to those found for NbOFFIVE. As there is no published data on the selectivity of the gases and MOF combinations used, it is difficult to draw comparisons with other works. However, the trends reported here lean towards the conclusion of the size sieving effect and strong interactions between the propyne and SIFSIX at low pressure range. A Q_{st} value of 68 kJ mol^{-1} at 0.003 bar was reported by Yang et al. [18] for SIFSIX, and was attributed to the effect of single-molecule trap and the strong interaction between the MOF and the gas molecules.

4.4. Modeling of the Equilibrium and Kinetic Adsorption for C₃H₄/C₃H₆ on Metal Organic Frameworks

Experimental data were fitted to isotherms in an effort to help predict the general behavior of the adsorbent adsorbate interactions and uptake values. Isotherms were divided into one-parameter isotherms, such as Langmuir and Freundlich, or a multicontent hybrid combination of the two models such as the Sips and Toth models, as explained in an earlier section. The affinity of the system for adsorption was indicated by the value of the calculated constants. In the case of Langmuir and Freundlich, the linearized form of the Equations (1) and (3) is used to estimate the equilibrium adsorption uptake amount (q_{sat}) under a given pressure and temperature system. It is also related to the maximum adsorbed amount Q . The experimental results obtained for both metal organic frameworks and the two gases were analyzed by regression analyses, and all model fits are represented in Figure 6. In the Freundlich model, a value of $1/n$ close to zero indicates a heterogeneous surface, while a value of n greater than 1 indicates strong affinity [41]. From the trends shown in Figure 6a,b, it can be seen that the two linearized models did not represent the adsorption data well, as reflected by the lowered AARD (Table 3) for the range of pressures for the SIFSIX and propyne systems. Having said that, both the Freundlich and Langmuir models represented the data between the other adsorbent adsorbate combinations. This may have been due to stronger monolayer type interactions between the propyne and SIFSIX compared to the NbOFFIVE gas system. Even in the case of propylene and SIFSIX, both isotherms managed to represent the data in a more accurate manner. It can also be seen that both models underestimated the experimental uptake data in most cases. This was more apparent at higher pressure regions, especially in the Nb gas adsorbent-adsorbate systems. Apart from SIFSIX/propyne, the isotherm models represented the data at lower pressure ranges. The Sips (combined Langmuir and Freundlich isotherm) and the Toth model regression fitting are given in Figure 6c,d. Both models offered a better fit of the experimental data over the entire range of pressures. Again, it can be seen that in the case of the SIFSIX and propyne combination, the Sips model was less accurate compared to the Toth model.

In addition to equilibrium and selectivity studies, information related to the adsorption system kinetics is key in designing of adsorption systems. The most reliable method of addressing the transient uptake curves is to use micropores diffusion models that are based on Fick's law of diffusion (Equation (9)). The modeled data are given in Figure 7, where the fractional uptake ratio is expressed as a function of time (solid lines are model-estimated values). It can be seen that the model fit the adsorption uptake data well at all combinations of metal organic frameworks and gases, indicating a diffusion based process. It can also be seen that the model fits the propyne and SIFSIX combination best. This was expected, given the availability of passage through the SIFSIX structure due to the suitability of the kinetic size of both the adsorbent and adsorbate. From Equation (9) and upon fitting of the experimental data, the values of D_c/r_c^2 were calculated and are reported in Table 3. It can be seen from Figure 7 that the value of the time constant of micropore diffusion D_c/r_c^2 increased with increase in temperature. In addition, the propyne time constant was smaller than that of propylene for both adsorbents owing to the ease of diffusion due to the size acceptance of propyne compared to that of propylene.

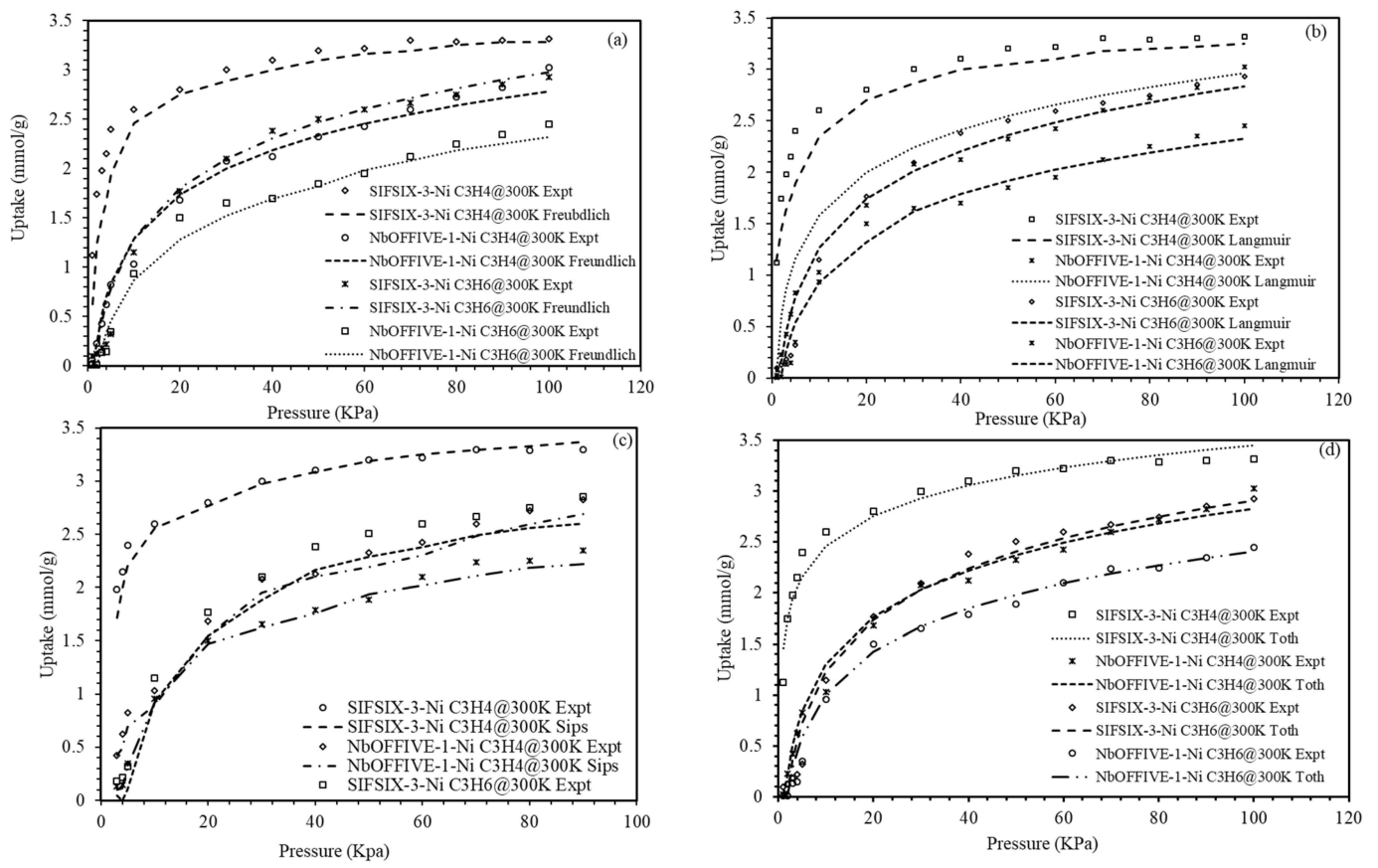


Figure 6. Fitted adsorption isotherms at temperatures of 300 K (a) Freundlich, (b) Langmuir, (c) Sips, (d) Toth.

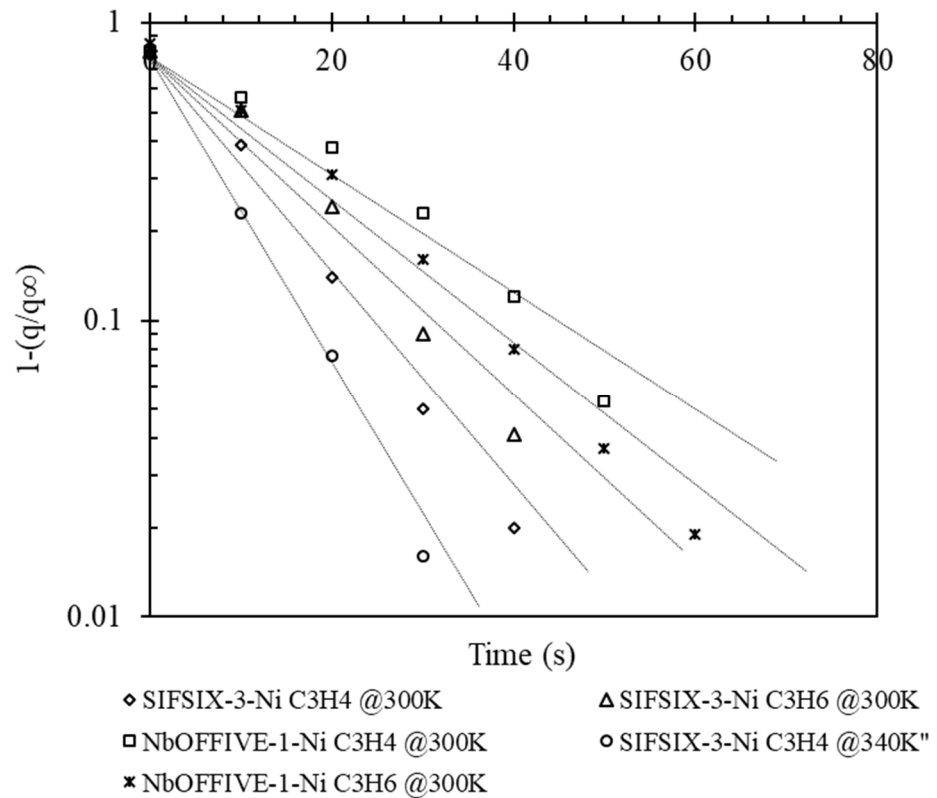


Figure 7. Fractional adsorption rate for C₃H₄/C₃H₆ on SIFSIX-3-Ni and NbOFFIVE-1-Ni.

4.5. Breakthrough and Cyclic Breakthrough Experiments

To confirm the validity of the kinetic effect and the ability and extent of the separation on the SIFSIX and NBOFFIVE metal organic frameworks, studies on binary mixtures of C_3H_4/C_3H_6 (10/90 *v/v*) were conducted. It can be clearly seen from the trends in Figure 8a that the heavier propylene molecules were eluted first from the column, in contrast to the lighter propyne molecules, upon adsorption on SIFSIX-3-Ni. Similar trends were found for the Nb gas combination (not shown). This also confirms earlier findings about the stronger bindings and affinities found between propyne and the SIFSIX adsorbent. The trends (Figure 8a) show that the breakthrough for propylene occurs after nearly 4–5 min and yields a 99.98% purity gas, while propyne was slowly eluted and becomes detectable in the outgas after nearly 16 min. This confirms the suitability of SIFSIX for the appropriate separation of C_3H_6/C_3H_4 systems. Accordingly, high purity propylene gas can be effectively separated and collected within the 10-min gap between the breakthrough of propyne and propylene from the column confirming the potential application of SIFSIX-3-Ni for the separation. Effective durability and recyclability are very important parameters in the selection and operation of adsorbent in gas separations. Eight cycles of adsorption and regeneration were conducted in order to examine the recyclability of the adsorbents and its effectiveness in repeated application. After each breakthrough test, the experimental breakthrough column was simply heated to around 423 K for 20 min [44] to allow the desorption of the gas adsorbed in the solid. Figure 8b shows the uptake ratios for eight consecutive cycles using the same experimental condition and adsorbent-adsorbate combinations. As can be seen, the adsorption capacity of the solids was not accepted with repeated use, confirming the suitability of solids for potential C_3H_4/C_3H_6 application.

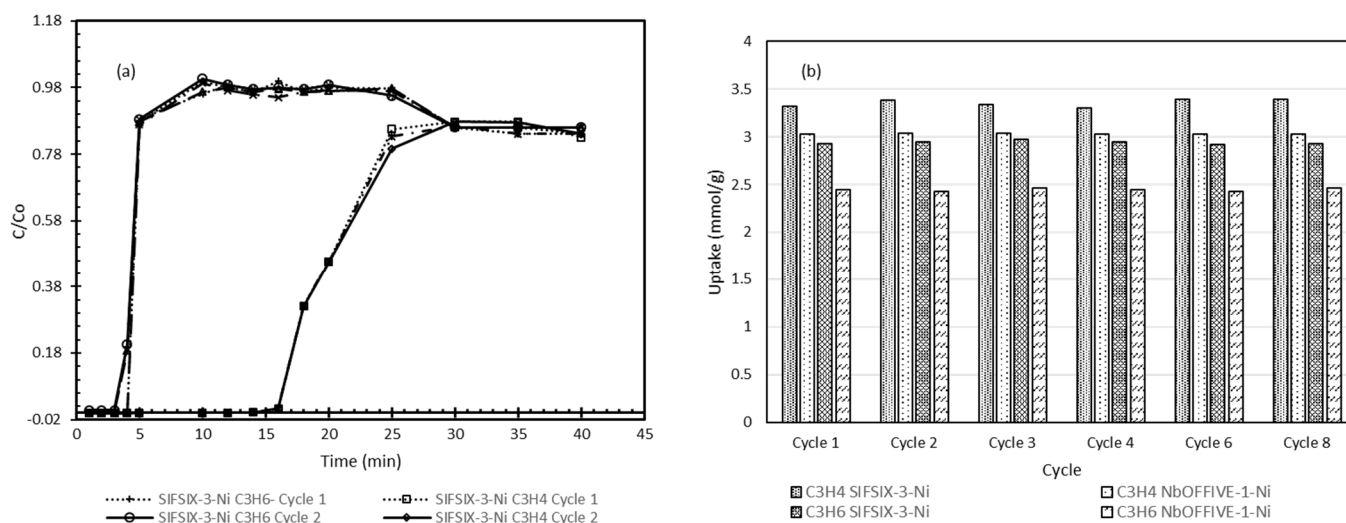


Figure 8. (a) Dynamic breakthrough curves for the SIFSIX and NbOFFIVE and C_3H_4/C_3H_6 systems at 300 K (4 cycles are shown); (b) uptake amounts of C_3H_4/C_3H_6 after 8 adsorption cycles at 300 K.

Table 3. Modeling isotherm statistical parameters, isosteric heats of adsorption and micropores diffusion time constants for MOFs and C₃H₄/ C₃H₆ at 300 K.

	SIFSIX-3-Ni		NbOFFIVE-1-Ni	
	C ₃ H ₄	C ₃ H ₈	C ₃ H ₄	C ₃ H ₈
Langmuir				
q _{sat} (mmol/g)	3.32	2.93	3.03	2.45
k _l	0.23	0.21	0.034	0.0022
R _l	0.82	0.65	0.74	0.62
AARD (%)	13.7	12.2	10.3	9.7
Freundlich				
n	0.298	0.228	0.265	0.2007
k _f	0.342	0.432	0.665	0.453
AARD (%)	9.2	8.5	6.8	6.3
Sips				
q _{sat} (mmol/g)	0.047	0.837	1.179	1.231
K _s (mmol/gbar)	0.0087	0.0076	0.0061	0.0052
m	0.067	0.025	0.0289	0.088
AARD (%)	2.3	1.7	3.2	2.1
Toth				
q _{sat} (mmol/g)	4.09	3.98	3.54	2.48
k _t	0.042	0.076	0.0342	0.066
n	0.203	0.019	0.187	0.0172
AARD(%)	0.03	0.04	0.05	0.04
Q _{st} (J/mol)	45.0	38.3	30.8	24.7
D _c /r _c ² (s ⁻¹)	9.34 × 10 ⁻³	5.23 × 10 ⁻³	6.14 × 10 ⁻³	4.12 × 10 ⁻³

5. Conclusions

This investigation reports the effective separation of propyne (C₃H₄) and propylene (C₃H₆) using the fluorinated metal organic framework, SIFSIX-3-Ni. The SIFSIX MOF showed a better adsorption capacity compared to another pyrazine based MOF (NbOFFIVE-1-Ni) under the same experimental conditions. Characterization of the adsorbents showed developed micropores and a stable structure with a BET area of around 248 m² g⁻¹. The maximum uptake recorded for the SIFSIX was in excess of 3.2 mmol g⁻¹ for C₃H₄ compared to 2.99 mmol g⁻¹ for C₃H₆. Size sieving and thermodynamic interactions were thought to be the main separation mechanisms, as indicated by the high isosteric heat of adsorption towards propyne on SIFSIX. The selectivity of propyne over propylene on the used metal organic frameworks can be attributed to kinetic (size exclusion) and thermodynamic (pore and surface interactions) combination. Isotherm models fitted the Toth model well for all combinations of solid metal organic frameworks and gases at the full applied range of temperatures. The smaller kinetic diameter of propyne and the strong interactions make its adsorption easier on SIFSIX-3-Ni and facilitate its possible application in the separation of propyne and propylene binary mixtures. A 10-min time difference between the breakthrough of C₃H₆ and the lighter C₃H₄ was evident from the dynamic breakthrough curves, indicating great potential for the application of SIFSIX-3-Ni for propyne/propylene separation.

Author Contributions: Conceptualization, M.K. and G.W.; methodology, M.K. and F.A.; software, M.K.; validation, M.K. and F.A.; formal analysis, M.K.; investigation, M.K.; data curation, M.K.;

writing—original draft preparation, M.K.; writing—review and editing, G.W. and F.A.; visualization, M.K.; supervision, M.K.; project administration, M.K. and F.A.; funding acquisition, M.K. and G.W. All authors have read and agreed to the published version of the manuscript.

Funding: Qatar National Research Fund under the National Priorities Research Program award number NPRP10-0107-170119.

Acknowledgments: The work was made possible by a grant from the Qatar National Research Fund under the National Priorities Research Program award number NPRP10-0107-170119. Its content are solely the responsibility of the authors and do not necessarily represent the official views of QNRF. The authors acknowledge the CLU unit at Qatar University for helping in sample analysis.

Conflicts of Interest: The authors declare no conflict of interest.

References

1. Wang, Y.; Zhao, D. Beyond Equilibrium: Metal–Organic Frameworks for Molecular Sieving and Kinetic Gas Separation. *Cryst. Growth Des.* **2017**, *17*, 2291–2308. [[CrossRef](#)]
2. Da Silva, F.A.; Rodrigues, A.E. Adsorption equilibria and kinetics for propylene and propane over 13X and 4A zeolite pellets. *Ind. Eng. Chem. Res.* **1999**, *38*, 2051–2057. [[CrossRef](#)]
3. Li, L.; Guo, L.; Zheng, F.; Zhang, Z.; Yang, Q.; Yang, Y.; Ren, Q.; Bao, Z. Calcium-Based Metal–Organic Framework for Simultaneous Capture of Trace Propyne and Propadiene from Propylene. *ACS Appl. Mater. Interfaces* **2020**, *12*, 17147–17154. [[CrossRef](#)] [[PubMed](#)]
4. Li, L.; Wen, H.-M.; He, C.; Lin, R.-B.; Krishna, R.; Wu, H.; Zhou, W.; Li, J.; Li, B.; Chen, B. A Metal–Organic Framework with Suitable Pore Size and Specific Functional Sites for the Removal of Trace Propyne from Propylene. *Angew. Chem.* **2018**, *130*, 15403–15408. [[CrossRef](#)]
5. Cui, W.; Hu, T.; Bu, X. Metal–Organic Framework Materials for the Separation and Purification of Light Hydrocarbons. *Adv. Mater.* **2020**, *32*, e1806445. [[CrossRef](#)]
6. Li, L.; Duan, Y.; Liao, S.; Ke, Q.; Qiao, Z.; Wei, Y. Adsorption and separation of propane/propylene on various ZIF-8 poly-morphs: Insights from GCMC simulations and the ideal adsorbed solution theory (IAST). *Chem. Eng. J.* **2020**, *386*, 123945. [[CrossRef](#)]
7. Martins, V.F.D.; Ribeiro, A.M.; Plaza, M.G.; Santos, J.C.; Loureiro, J.M.; Ferreira, A.F.P. Gas-phase simulated moving bed: Propane/propylene separation on 13X zeolite. *J. Chromatogr. A* **2015**, *1423*, 136–148. [[CrossRef](#)]
8. Mundstock, A.; Wang, N.; Friebe, S.; Caro, J. Propane/propene permeation through Na-X membranes: The interplay of separation performance and pre-synthetic support functionalization. *Microporous Mesoporous Mater.* **2015**, *215*, 20–28. [[CrossRef](#)]
9. Kim, J.; Hong, S.H.; Park, D.; Chung, K.; Lee, C. Separation of propane and propylene by desorbent swing adsorption using zeolite 13X and carbon dioxide. *Chem. Eng. J.* **2021**, *410*, 128276. [[CrossRef](#)]
10. Abedini, H.; Shariati, A.; Khosravi-Nikou, M.R. Adsorption of propane and propylene on M-MOF-74 (M = Cu, Co): Equilibrium and kinetic study. *Chem. Eng. Res. Des.* **2020**, *153*, 96–106. [[CrossRef](#)]
11. Dobladez, J.A.D.; Maté, V.I.Á.; Torrellas, S.Á.; Larriba, M. Separation of the propane propylene mixture with high recovery by a dual PSA process. *Comput. Chem. Eng.* **2020**, *136*, 106717. [[CrossRef](#)]
12. Grande, C.A.; Gascon, J.; Kapteijn, F.; Rodrigues, A.E. Propane/propylene separation with Li-exchanged zeolite 13X. *Chem. Eng. J.* **2010**, *160*, 207–214. [[CrossRef](#)]
13. Jorge, M.; Lamia, N.; Rodrigues, A.E. Molecular simulation of propane/propylene separation on the metal–organic framework CuBTC. *Colloids Surf. A Physicochem. Eng. Asp.* **2010**, *357*, 27–34. [[CrossRef](#)]
14. Lamia, N.; Wolff, L.; Leflaive, P.; Gomes, P.S.; Grande, C.A.; Rodrigues, A.E. Propane/Propylene Separation by Simulated Moving Bed I. Adsorption of Propane, Propylene and Isobutane in Pellets of 13X Zeolite. *Sep. Sci. Technol.* **2007**, *42*, 2539–2566. [[CrossRef](#)]
15. Li, L.; Lin, R.-B.; Wang, X.; Zhou, W.; Jia, L.; Li, J. Kinetic separation of propylene over propane in a microporous metal-organic framework. *Chem. Eng. J.* **2018**, *354*, 977–982. [[CrossRef](#)]
16. Plaza, M.; Ribeiro, A.; Ferreira, A.; Santos, J.; Lee, U.-H.; Chang, J.-S. Propylene/propane separation by vacuum swing adsorption using Cu-BTC spheres. *Sep. Purif. Technol.* **2012**, *90*, 109–119. [[CrossRef](#)]
17. Wang, S.; Zhang, Y.; Tang, Y.; Wen, Y.; Lv, Z.; Liu, S.; Li, X.; Zhou, X. Propane-selective design of zirconium-based MOFs for propylene purification. *Chem. Eng. Sci.* **2020**, *219*. [[CrossRef](#)]
18. Yang, L.; Cui, X.; Yang, Q.; Qian, S.; Wu, H.; Bao, Z. A Single-Molecule Propyne Trap: Highly Efficient Removal of Propyne from Propylene with Anion-Pillared Ultramicroporous Materials. *Adv. Mater.* **2018**, *30*, 1705374. [[CrossRef](#)]
19. Yang, L.; Cui, X.; Zhang, Y.; Yang, Q.; Xing, H. A highly sensitive flexible metal–organic framework sets a new benchmark for separating propyne from propylene. *J. Mater. Chem. A* **2018**, *6*, 24452–24458. [[CrossRef](#)]
20. Das, M.C.; Guo, Q.; He, Y.; Kim, J.; Zhao, C.-G.; Hong, K.; Xiang, S.; Zhang, Z.; Thomas, K.M.; Krishna, R.; et al. Interplay of Metalloligand and Organic Ligand to Tune Micropores within Isostructural Mixed-Metal Organic Frameworks (M'MOFs) for Their Highly Selective Separation of Chiral and Achiral Small Molecules. *J. Am. Chem. Soc.* **2012**, *134*, 8703–8710. [[CrossRef](#)]
21. Li, L.; Lin, R.-B.; Krishna, R.; Wang, X.; Li, B.; Wu, H. Flexible–robust metal–organic framework for efficient removal of propyne from propylene. *J. Am. Chem. Soc.* **2017**, *139*, 7733–7736. [[CrossRef](#)] [[PubMed](#)]

22. Wang, X.; Krishna, R.; Li, L.; Wang, B.; He, T.; Zhang, Y.-Z.; Li, J.-R.; Li, J. Guest-dependent pressure induced gate-opening effect enables effective separation of propene and propane in a flexible MOF. *Chem. Eng. J.* **2018**, *346*, 489–496. [[CrossRef](#)]
23. Bulánek, R.; Koudelková, E.; de Oliveira Ramos, F.S.; Trachta, M.; Bludský, O.; Rubeš, M. Experimental and theoretical study of propene adsorption on alkali metal exchanged FER zeolites. *Microporous Mesoporous Mater.* **2019**, *280*, 203–210. [[CrossRef](#)]
24. Li, X.; Shen, W.; Zheng, A. The influence of acid strength and pore size effect on propene elimination reaction over zeolites: A theoretical study. *Microporous Mesoporous Mater.* **2019**, *278*, 121–129. [[CrossRef](#)]
25. Liu, G.; Labreche, Y.; Chernikova, V.; Shekhah, O.; Zhang, C.; Belmabkhout, Y.; Eddaoudi, M.; Koros, W.J. Zeolite-like MOF nanocrystals incorporated 6FDA-polyimide mixed-matrix membranes for CO₂/CH₄ separation. *J. Membr. Sci.* **2018**, *565*, 186–193. [[CrossRef](#)]
26. Yilmaz, G.; Keskin, S. Molecular modeling of MOF and ZIF-filled MMMs for CO₂/N₂ separations. *J. Membr. Sci.* **2014**, *454*, 407–417. [[CrossRef](#)]
27. Elsaidi, S.K.; Mohamed, M.H.; Banerjee, D.; Thallapally, P.K. Flexibility in Metal–Organic Frameworks: A fundamental understanding. *Coord. Chem. Rev.* **2018**, *358*, 125–152. [[CrossRef](#)]
28. Li, H.; Li, L.; Lin, R.-B.; Zhou, W.; Zhang, Z.; Xiang, S.; Chen, B. Porous metal-organic frameworks for gas storage and separation: Status and challenges. *EnergyChem* **2019**, *1*, 100006. [[CrossRef](#)]
29. Zhang, J.; Chen, Z. Metal-organic frameworks as stationary phase for application in chromatographic separation. *J. Chromatogr. A* **2017**, *1530*, 1–18. [[CrossRef](#)]
30. Khraisheh, M.; Mukherjee, S.; Kumar, A.; Al Momani, F.; Walker, G.; Zaworotko, M.J. An overview on trace CO₂ removal by advanced physisorbent materials. *J. Environ. Manag.* **2020**, *255*, 109874. [[CrossRef](#)]
31. Madden, D.; Albadarin, A.B.; O’Nolan, D.; Cronin, P.; Perry, I.V.J.J.; Solomon, S. Metal-Organic Material Polymer Coatings for Enhanced Gas Sorption Performance and Hydrolytic Stability Under Humid Conditions. *ACS Appl. Mater. Interfaces* **2020**. [[CrossRef](#)] [[PubMed](#)]
32. Madden, D.G.; O’Nolan, D.; Chen, K.-J.; Hua, C.; Kumar, A.; Pham, T.; Forrest, K.A.; Space, B.; Perry, J.J.; Khraisheh, M.; et al. Highly selective CO₂ removal for one-step liquefied natural gas processing by physisorbents. *Chem. Commun.* **2019**, *55*, 3219–3222. [[CrossRef](#)]
33. Cadiau, A.; Adil, K.; Bhatt, P.; Belmabkhout, Y.; Eddaoudi, M. A metal-organic framework-based splitter for separating propyl-ene from propane. *Science* **2016**, *353*, 137–140. [[CrossRef](#)]
34. Khraisheh, M.; Almomani, F.; Walker, G. Solid Sorbents as a Retrofit Technology for CO₂ Removal from Natural Gas Under High Pressure and Temperature Conditions. *Sci. Rep.* **2020**, *10*, 1–12. [[CrossRef](#)]
35. Ullah, S.; Bustam, M.A.; Al-Sehemi, A.G.; Assiri, M.A.; Abdul Kareem, F.A.; Mukhtar, A. Influence of post-synthetic graphene oxide (GO) functionalization on the selective CO₂/CH₄ adsorption behavior of MOF-200 at different temperatures; an experimental and adsorption isotherms study. *Microporous Mesoporous Mater.* **2020**, *296*, 110002. [[CrossRef](#)]
36. Ullah, S.; Bustam, M.A.; Assiri, M.A.; Al-Sehemi, A.G.; Gonfa, G.; Mukhtar, A.; Kareem, F.A.A.; Ayoub, M.; Saqib, S.; Mellon, N.B. Synthesis and characterization of mesoporous MOF UMCM-1 for CO₂/CH₄ adsorption; an experimental, isotherm modeling and thermodynamic study. *Microporous Mesoporous Mater.* **2020**, *294*, 109844. [[CrossRef](#)]
37. Weston, M.H.; Colón, Y.J.; Bae, Y.-S.; Garibay, S.J.; Snurr, R.Q.; Farha, O.K.; Hupp, J.T.; Nguyen, S.T. High propylene/propane adsorption selectivity in a copper(catecholate)-decorated porous organic polymer. *J. Mater. Chem. A* **2013**, *2*, 299–302. [[CrossRef](#)]
38. Kim, A.-R.; Yoon, T.-U.; Kim, E.-J.; Yoon, J.W.; Kim, S.-Y.; Yoon, J.W. Facile loading of Cu (I) in MIL-100 (Fe) through redox-active Fe (II) sites and remarkable propylene/propane separation performance. *Chem. Eng. J.* **2018**, *331*, 777–784. [[CrossRef](#)]
39. Bhatt, P.M.; Belmabkhout, Y.; Cadiau, A.; Adil, K.; Shekhah, O.; Shkurenko, A.; Barbour, L.J.; Eddaoudi, M. A Fine-Tuned Fluorinated MOF Addresses the Needs for Trace CO₂ Removal and Air Capture Using Physisorption. *J. Am. Chem. Soc.* **2016**, *138*, 9301–9307. [[CrossRef](#)]
40. Kumar, A.; Hua, C.; Madden, D.G.; O’Nolan, D.; Chen, K.-J.; Keane, L.-A.J.; Perry, J.J.; Zaworotko, M.J. Hybrid ultramicroporous materials (HUMs) with enhanced stability and trace carbon capture performance. *Chem. Commun.* **2017**, *53*, 5946–5949. [[CrossRef](#)]
41. Ullah, S.; Bustam, M.A.; Assiri, M.A.; Al-Sehemi, A.G.; Sagir, M.; Abdul Kareem, F.A. Synthesis, and characterization of metal-organic frameworks -177 for static and dynamic adsorption behavior of CO₂ and CH₄. *Microporous Mesoporous Mater.* **2019**, *288*, 109569. [[CrossRef](#)]
42. Lin, Z.-T.; Liu, Q.-Y.; Yang, L.; He, C.-T.; Li, L.; Wang, Y.-L. Fluorinated Biphenyldicarboxylate-Based Metal–Organic Framework Exhibiting Efficient Propyne/Propylene Separation. *Inorg. Chem.* **2020**, *59*, 4030–4036. [[CrossRef](#)]
43. Li, L.; Krishna, R.; Wang, Y.; Yang, J.; Wang, X.; Li, J. Exploiting the gate opening effect in a flexible MOF for selective adsorption of propyne from C1/C2/C3 hydrocarbons. *J. Mater. Chem. A* **2016**, *4*, 751–755. [[CrossRef](#)]
44. Wu, H.; Yuan, Y.; Chen, Y.; Xu, F.; Lv, D.; Wu, Y. Efficient adsorptive separation of propene over propane through a pillar-layer cobalt-based metal–organic framework. *AIChE J.* **2020**, *66*, e16858. [[CrossRef](#)]